CrossMark

Electromagnetism / Électromagnétisme

Metamaterial-based "sabre" antenna

Antenne « sabre » à base de métamatériaux

Habiba Hafdallah Ouslimani [a,*], Tangjie Yuan [a], Houcine Kanane [a,b], Alain Priou [a], Gérard Collignon [c], Guillaume Lacotte [c]

[a] *Université Paris-Ouest – Nanterre – La Défense, Energetic Mechanic Electromagnetic Lab LEME (EA-4416), Group of Metamaterial Microwave and Optical Applications, 50, rue de Sèvres, 92410 Ville-d'Avray, France*
[b] *University Mouloud Maameri of Tizi-Ouzou – UMMTO, Algeria*
[c] *INEO Défense, route Militaire Nord, ZA Louis-Bréguet, CS 80526, 78140 Vélizy-Villacoublay, France*

A B S T R A C T

The "sabre" antenna is an array of two monopole elements, vertically polarized with omnidirectional radiation patterns, and placed on either side of a composite material on the tail of an airplane. As an in-phase reflector plane, the antenna uses a compact dual-layer high-impedance surface (DL-HIS) with offset mushroom-like Sivenpiper square shape unit cells. This topology allows one to control both operational frequency and bandgap width, while reducing the total height of the antenna to under $\lambda_0/36$. The designed antenna structure has a wide bandwidth higher than 24% around 1.4 GHz. The measurements and numerical simulations agree very well.

© 2014 Académie des sciences. Published by Elsevier Masson SAS. All rights reserved.

R É S U M É

L'antenne « sabre » est une antenne réseau formée de deux monopôles à polarisation verticale et rayonnement omnidirectionnel, placées de part et d'autre d'un matériau composite sur la dérive d'un avion. L'antenne utilise, comme plan réflecteur en phase, une surface haute impédance (SHI) formée d'une double-couche de cellules champignons de « type Sivenpiper » carrées décalées. La topologie choisie permet de contrôler simultanément la fréquence centrale et la largeur de bande utile pour une compacité optimum, avec une hauteur totale inférieure à $\lambda_0/36$. La structure antennaire présente une bande passante supérieure à 24% autour de 1,4 GHz. Les mesures et les simulations numériques sont en bon accord.

© 2014 Académie des sciences. Published by Elsevier Masson SAS. All rights reserved.

---

* Tel.: +33 (0)1 40 97 41 10; fax: +33 (0)1 40 97 41 10.
  E-mail address: habiba.ouslimani@u-paris10.fr (H. Hafdallah Ouslimani).
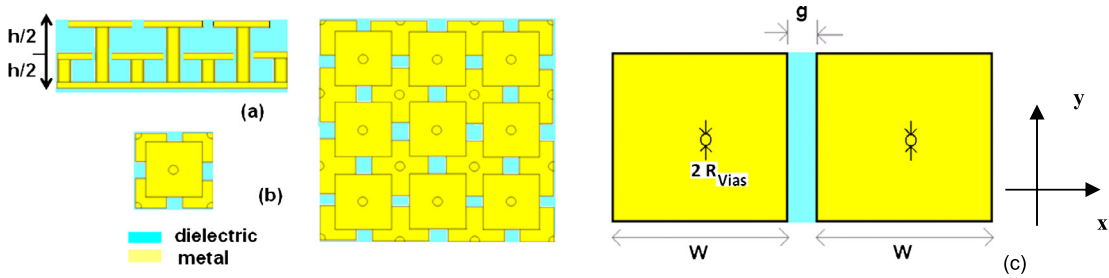
Fig. 1. (Color online.) Dual-layer metamaterial structure: (a) square patches with offset metalized vias (side view) and (b) and (c) top view of unit cells and the dimensions.

Fig. 1. (Couleur en ligne.) Structure haute impédance métamatériau double couche : (a) vue de côté de la structure avec les « vias » métalliques, (b) et (c) vue de dessus montrant les cellules élémentaires carrées décalées et leurs dimensions.

Table 1
Dimensions of the mushroom dual-layer HIS (Fig. 1).

Tableau 1
Dimensions de la double couche « mushroom-like » HIS (Fig. 1).

| Symbol	Name	Dimensions	Normalized dimensions
W	Metallic square patch	33.4 mm	$0.15\lambda_0$
g	Gap between adjacent patches	4.6 mm	$0.02\lambda_0$
h	Substrate thickness	5.08 mm	$0.022\lambda_0$
R_{vias}	VIAS radius	1.3 mm	$0.005\lambda_0$
a	Distance monopole to DL-HIS	1.27 mm	$0.006\lambda_0$
$(h+a)$	Total height of the designed antenna	6.35 mm	$0.028\lambda_0$
S	Ground plane dimensions	266 mm × 266 mm	$1.15\lambda_0 \times 1.15\lambda_0$

1. Introduction

Aircraft and all holders are generally equipped with antennal structures and/or radar functions that promote ground communications or satellite link (VHF, HF, SATCOM), navigation devices (ILS, MLS, DME, GPS, VOR, Radio Altimeter) and monitoring (ATC TICAS) [1–5]. Effective integration of these antenna systems is made possible only if we have implemented materials which are compact, compatible with composite technologies, enough flexible, smart, configurable or reconfigurable, able to adapt the holder(s) structure(s) in specific locations. At present, there is a global race to reduce the number of antennal structures on board, reducing their size and allowing their integration as well as in flat, curve and deformable areas [1–5]. The interest in low-profile antennas for aeronautic and aerospace applications is growing. Engineered metamaterial (also called artificial material) and especially electromagnetic bandgap (EBG) structures have been successfully used as artificial ground planes for antennas with improved properties [6–12]. The designed antennas exhibit attractive features: total height reduction ($\ll 0.1\lambda$) and VSWR bandwidth, directivity and gain enhancement [6–12].

We present in this paper, for the first time, the design, optimization and characterization of a "sabre" antenna based on low-profile monopole elements. The "sabre-type" is an array of two identical elements, placed on either side on the tail of an airplane. The monopole antenna has a very thin total height $\approx \lambda_0/36$ in comparison to the operating wavelength (λ_0) calculated at 1.3 GHz. The designed metamaterial (MTM) structure is based on a dual-layer of offset mushroom-like periodic pattern baked by a metallic ground plane. It is used a reflector artificial ground plane with a height of $\approx \lambda_0/40$. The antennal structures have been designed and optimized by numerical simulations [13] and validated experimentally by the characterization of the fabricated prototypes. The antennas present a broadband feature (Bw > 24%) and high gain (~8 dB) at 1.4 GHz.

2. Metamaterial structure

The metamaterial unit cell is a "mushroom-like" square patch connected to the ground plane with a metalized vias [14–17]. The critical parameters illustrated in Fig. 1 are: the patch size ($W \times W$), the gap or the distance between adjacent patches (g), the diameter of the vias ($2 \times R_{\text{vias}}$), the height (h) and the material of the substrate. The periodicity is $p = W + g$ (Table 1).

The designed high-impedance surface (HIS) is a dual-layer of two offset unit cells shown in Fig. 1a–b. This topology [6–12] allows us to control the total height of the metamaterial antenna (subwavelength) as well as the resonant frequency, and to expand its bandwidth (up to 24% in this case) (Fig. 1a). The numerical simulations show the superiority of the dual layer in front of a "standard" single-layer "mushroom-like" square patches, meanwhile all the other parameters (dimensions and dielectric substrate permittivity and height) are kept identical (see details in Section 2).

(a)   (b)
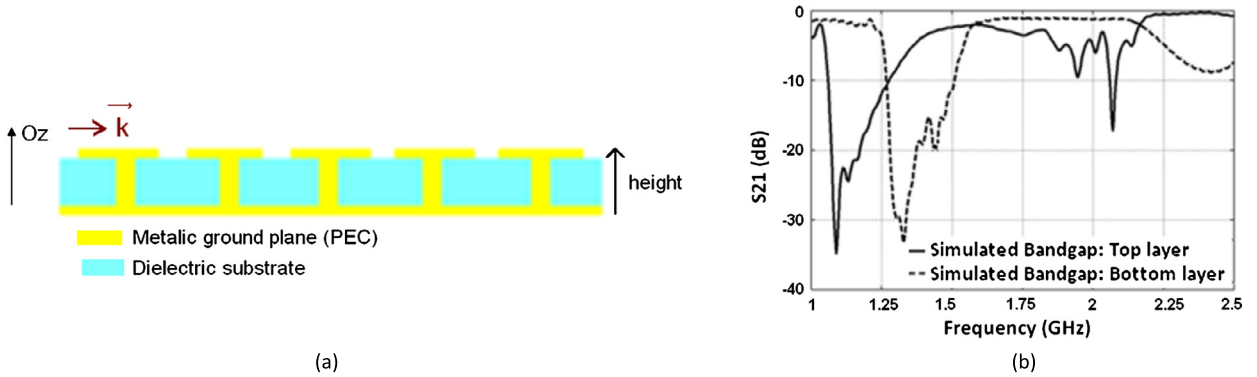
Fig. 2. (Color online.) (a) Simulated structure with two different heights, and (b) simulated surface wave bandgap (transmission S_{21} (dB)) determined for each mushroom-like HIS layer (top layer and bottom layer separately). For each layer, the interruption of the surface wave propagation corresponds to its bandgap.

Fig. 2. (Couleur en ligne.) (a) Structure simulée pour deux hauteurs différentes et (b) paramètre de transmission des ondes de surface simulé pour les couches métamatériaux séparément. On voit l'interruption de propagation des ondes de surface et le bandgap de chaque couche.
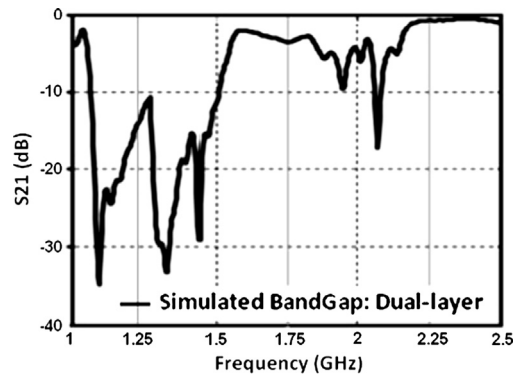
Fig. 3. Surface wave S_{21} parameter simulated across the entire dual-layer HIS structure (Table 1).

Fig. 3. Simulation du paramètre de transmission S_{21} (dB) des ondes de surface à travers la structure DL-HIS complète (Tableau 1).

The numerical model and full-wave simulations of the metamaterial structure and antennas are performed using CST MI-CROWAVE STUDIO SUITE™ (CST MWS) [13] based on the Finite Integration Technique (FIT) and using a tetrahedral meshing grid system to accurately model the complex antenna structure.

The dielectric substrate is the Rogers RT/Duroid® RT5880 LZ with a relative permittivity of 1.96 and a dielectric loss tangent $\tan\delta = 0.0019$.

Table 1 gives a summary of the final dimensions of the metasurface. λ_0 is calculated at 1.3 GHz.

Numerical studies and parametrical optimizations are performed on the designed mushroom dual-layer structure (DL-HIS) in order to determine a suitable frequency range, i.e. approximately from 1.1 GHz to 1.5 GHz. Complementary approaches are used [14–19]. The aim is to converge toward the suitable operational bandwidth with the optimum lowest thickness for low-profile antenna design.

We notice that for a low-profile antenna, complicated and strong interactions occur between the antenna element and the metamaterial ground plane; the operational bandwidth is defined only by the frequency range where the antenna radiates efficiently [17].

2.1. Surface wave bandgap

The surface wave signal across the MTM surface (Fig. 2a) is calculated using a quasi-TEM propagation mode [18]. Fig. 2b displays the simulated surface wave bandgap for each layer (Fig. 2a) of the mushroom-like structure. The top layer with a height $h = 0.022\lambda_0$ presents a resonant frequency around 1.1 GHz and a bandgap of ∼18.3% (for a transmitted signal S_{21} below −10 dB). The bottom layer, which has a half height $h/2 = 0.011\lambda_0$, presents a resonant frequency around 1.35 GHz with a bandwidth of ∼18% (Fig. 2b). For these two simulations, the parameters W, g, R_{vias} and dielectric properties are unchanged (see Table 1).

Fig. 3 gives the numerical result of the surface wave transmitted parameter (S_{21}) simulated over the entire DL-HIS structure. It appears that the previous bandgaps (Fig. 2) overlap, giving rise to wider bandgap; which goes from 1.06 GHz to 1.5 GHz with a central frequency at ∼1.3 GHz.
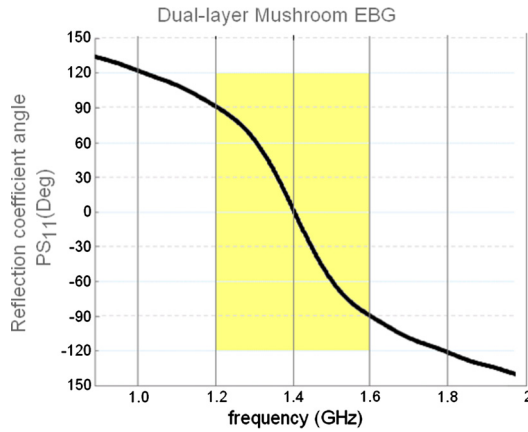
Fig. 4. (Color online.) Simulated reflection phase (PS$_{11}$) of the DL-HIS under incident plane wave. The in-phase area (dashed surface) defined for a phase between ±90° varies from 1.2 GHz to 1.6 GHz (central frequency 1.4 GHz).

Fig. 4. (Couleur en ligne.) Phase du coefficient de réflexion (PS$_{11}$) simulé à la surface de la DL-HIS sous incidence normale. La phase évoluant entre ±90° (partie colorée de la courbe) est entre 1,2 GHz et 1,6 GHz (fréquence centrale 1,4 GHz). Cela correspond au domaine de fréquence dit « bandgap », où la structure métamatériau est en phase.
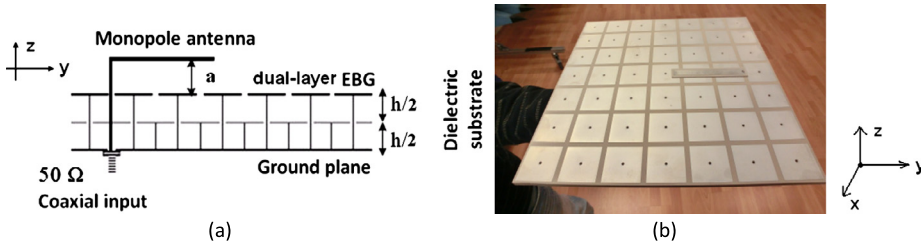
Fig. 5. Designed metamaterial monopole antenna: (a) schematic side view of the dual-layer "mushroom-like" HIS and the monopole element, and (b) the fabricated prototype (dimensions in Table 1).

Fig. 5. Structure de l'antenne monopole métamatériau développée : (a) vue en coupe de la structure de type « mushroom » carrée double couche et (b) prototype fabriqué de l'antenne métamatériau (dimensions dans le Tableau 1).

2.2. Reflection phase of the DL-HIS for a normally incident plane wave

Fig. 4 gives the simulated result of the reflection phase (PS$_{11}$) of the DL-HIS determined for incident plane wave (incidence angle $\vartheta = 0$). The phase varies from $-180°$ to $180°$ with a phase equal to zero (PS$_{11} = 0$) at the $f_0 = 1.4$ GHz. At this frequency, the surface behaves like a magnetic wall (or artificial magnetic conductor AMC) with a total in-phase reflection ($S_{11} = +1$). This is why it is also called high-impedance surface (HIS). As mentioned before, the operational bandwidth of the antenna is determined by the interactions between the antenna and the metasurface [18]. Hence, if one takes the $0° \pm 90°$ reflection phase as the criterion of the HIS surface, the frequency interval lies from 1.2 GHz to 1.6 GHz, corresponding to a fractional bandwidth of 24%. If one chooses rather the $90° \pm 45°$ reflection phase as the criterion (as discussed in [18]), the frequency region of interest varies from 0.9 GHz to 1.35 GHz (Fig. 4).

In Section 3, simulation results on the interaction between the antenna element and the compact DL-HIS ground plane will be presented. The distance in between is highly sensitive and hence requires a careful optimization.

3. Design of the metamaterial-based monopole antenna

The topology of the designed metamaterial-based monopole antenna is shown in Fig. 5a. It consists of a "mushroom-like" dual-layer structure which plays the role of an artificial in-phase ground plane (height h) and a monopole antenna placed at a distance a from the substrate. Fig. 5b shows a photograph of the manufactured prototype.

Fig. 6a shows a comparison of the measured and simulated voltage stationary wave ratio (VSWR) of the antenna. Fig. 6b gives the magnitude of the measured reflection coefficient, S_{11} (dB). Despite a slightly frequency shift between the measured and the simulated results, we observe an excellent agreement of their waveforms and shapes.

As Fig. 6a shows, the numerical simulation evidences a resonant frequency at 1.35 GHz and a bandwidth (VSWR ≤ 2) of 324 MHz from 1.194 GHz to 1.518 GHz, which corresponds to a fractional bandwidth of 24%. This agrees well with the surface wave bandgap result in Fig. 3. The measurements (Fig. 6a–b) show a resonant frequency at 1.4 GHz (shift of 50 MHz)
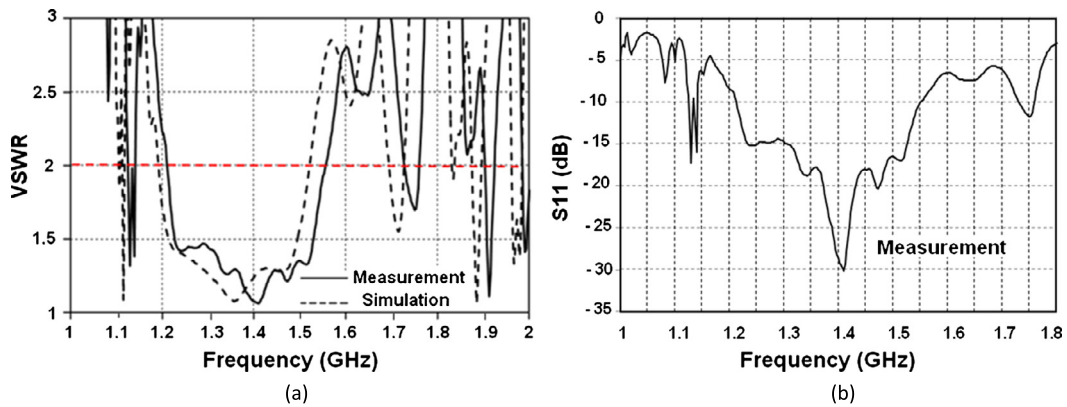
Fig. 6. (a) Comparison of the measured and simulated VSWR of the designed antenna and (b) the magnitude of the measured reflection coefficient S_{11} (dB) (dimensions in Table 1).

Fig. 6. (a) Comparaison des résultats de mesure et de simulation du taux d'ondes stationnaires (VSWR) de l'antenne monopole métamatériau et (b) amplitude S_{11} (dB) du coefficient de réflexion de l'antenne (dimensions dans le Tableau 1).

and a bandwidth of 337 MHz from 1.213 GHz to 1.55 GHz, which corresponds to a fractional bandwidth of 24,4%. Hence the measured bandwidth is larger than that expected by the simulation and fits better with the calculated bandwidth using the reflection phase PS_{11} in Fig. 5.

These results demonstrate clearly the benefit impact of the DL-HIS on the antenna performances. Thanks to the metamaterial ground plane, the designed DL-HIS based antenna is ultra-compact, with a total height $(h + a)$ of only $\approx \lambda_0/36$. It is well matched over a broadband frequency range (337 MHz) and exhibits a large radiation gain (see results below). In comparison, Fig. 7a presents two additional simulated results, where the ground plane is a perfect metallic conductor (PEC). The total distance between the antenna and the PEC $(h + a)$ is respectively $\sim\lambda_0/36$ and $\sim\lambda_0/7$, where λ_0 is calculated for $f = 1.3$ GHz.

– For a height of $(h + a) \approx \lambda_0/36$, the antenna over a PEC ground plane is completely non-matched and behaves almost like a capacitive circuit.
– For a height of $(h + a) \approx \lambda_0/7$, the antenna has a resonant frequency around 1.3 GHz and, as shown in Fig. 7b, its bandwidth (S_{11} (dB) < -10) goes from 1.25 GHz to 1.33 GHz, corresponding to a fractional bandwidth of 6%.

Fig. 7b presents a comparison of the reflected signal (S_{11} (dB)) between the DL-HIS antenna; the height $(h + a) \approx \lambda_0/36$ (measured and simulated results) and the PEC antenna $(h + a) \approx \lambda_0/7$ (simulated results).

Finally, Fig. 8 gives the surface wave or surface current that propagates on the top and bottom metallic surfaces of the DL-HIS structure. It depicts the interactions between the monopole antenna and the metamaterial surface at the resonant frequency $f_0 = 1.4$ GHz. The bandgap of the mushroom-like structure suppress the propagation of the induced current, which is limited to the first closer unit cells around the antenna.

Fig. 9 depicts the simulated results showing the role of the DL-HIS substrate in controlling the resonant frequency and the bandwidth of the designed antenna. It presents a comparative study between two metamaterial-based antennas: a dual layer of offset mushroom-like HIS (DL-HIS) and a single-layer of mushroom-like HIS (SL-HIS). The substrate height h remains unchanged ($0.023\lambda_0$).

In contrast, the distance a (Fig. 5a) between the monopole element and the substrate is modified. Fig. 9a presents the reflection magnitude; S_{11} (dB) of the DL-HIS antenna when the distance a takes the following values: $\lambda_0/1000$, $6\lambda_0/1000$ and $11\lambda_0/1000$ (λ_0 is the wavelength at 1.3 GHz). Similarly, Fig. 9b shows the reflection magnitude for the SL-HIS with a varying from $2\lambda_0/100$ to $4\lambda_0/100$.

For a judicious value of the distance a, a good matching impedance ($S_{11} < -10$ dB) can be obtained for the two antennas (Fig. 9). However, the frequency behaviors of the two structures are completely different. The DL-HIS antenna central frequency (f_0) and the operational bandwidth (Bw) are very sensitive to the parameter a. In contrast, the central frequency and bandwidth of the SL-HIS antenna are almost stationary for $0.03\lambda_0 \pm 0.01\lambda_0$ and do not change significantly. Tables 2 and 3 summarize the variations of f_0 and Bw with the parameter a, respectively, for the DL-HIS and SL-HIS antennas.

For the DL-HIS antenna (Fig. 9a), the distance of interaction between the metasurface and the monopole antenna is very low ($\sim a/\lambda_0 = 0.006$, Fig. 9a). It is $\sim a/\lambda_0 = 0.03$ for the SL-HIS ground plane (Fig. 9b), which represents a factor 5:1.

In conclusion, the DL-HIS ground plane has an excellent feature in designing very compact "low-profile" antennas.

(a)

(b)
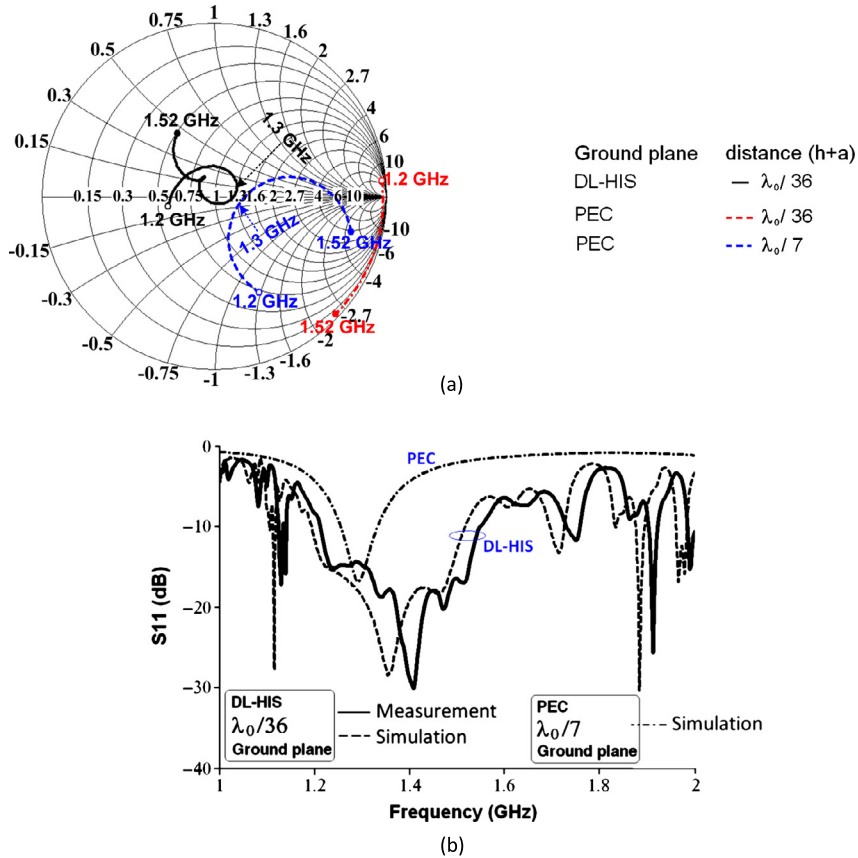
Fig. 7. (Color online.) (a) Reflection coefficient S_{11} (Smith chart) for three studied antennas with and without metamaterial ground plane and for two total heights (see inset legend), and (b) measured and simulated S_{11} (dB) of the $\lambda_0/36$ DL-HIS antenna in comparison with the simulated S_{11} (dB) of a PEC, $\lambda_0/7$ antenna.

Fig. 7. (Couleur en ligne.) (a) Coefficient de réflexion S_{11} (représentation polaire de Smith) pour les antennes étudiées avec et sans métamatériau et pour deux hauteurs différentes (voir la légende in situ) et (b) comparaison du module du coefficient de réflexion S_{11} (dB), mesuré et simulé dans le cas de l'antenne métamatériau actuelle (DL-HIS, $\lambda_0/36$) et simulé dans le cas d'une antenne placée à une hauteur $\lambda_0/7$ sur un plan métallique parfaitement conducteur (PEC).
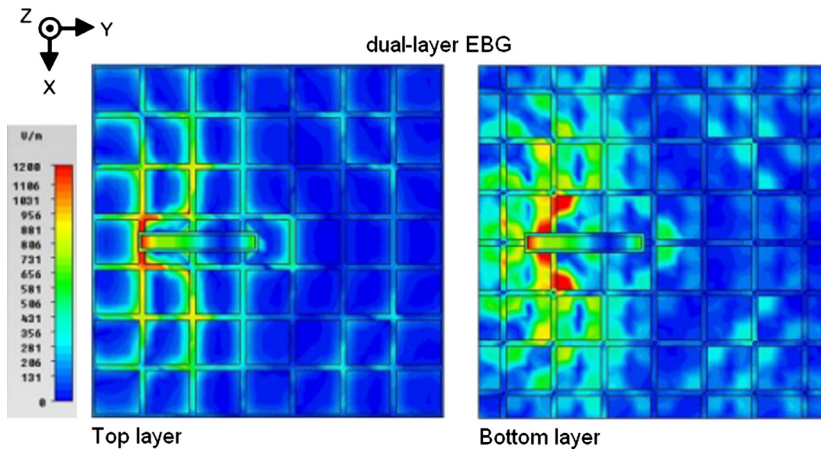

Fig. 8. (Color online.) Surface current distribution on the top and bottom plates of the DL-HIS at 1.4 GHz.

Fig. 8. (Couleur en ligne.) Distribution des courants de surface sur les deux couches métamatériaux de la structure DL-HIS à 1,4 GHz.
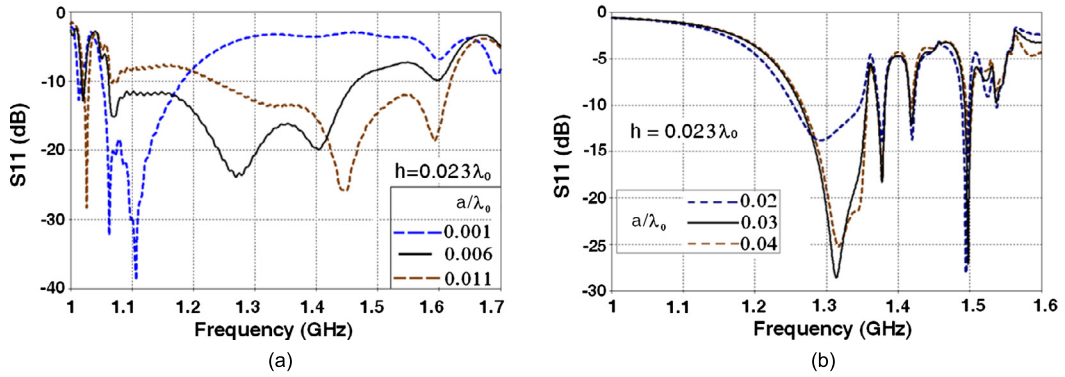
Fig. 9. (Color online.) Comparisons of the simulated reflection coefficient S_{11} of the two antennas with different HIS substrates: (a) dual-layer mushroom-like HIS antenna and (b) single-layer "standard" mushroom-like HIS antenna. The distance a can be adjusted so as to better adapt the antenna.

Fig. 9. (Couleur en ligne.) Comparaison entre les coefficients de réflexion S_{11} (dB) pour deux antennes monopoles ayant des substrats métamatériaux différents : (a) le substrat est une surface haute impédance double couche (DL-HIS étudié dans ce papier) et (b) le substrat est une structure haute impédance « standard » simple couche (SL-HIS). Le paramètre a est ajusté pour obtenir une bonne adaptation de l'antenne.
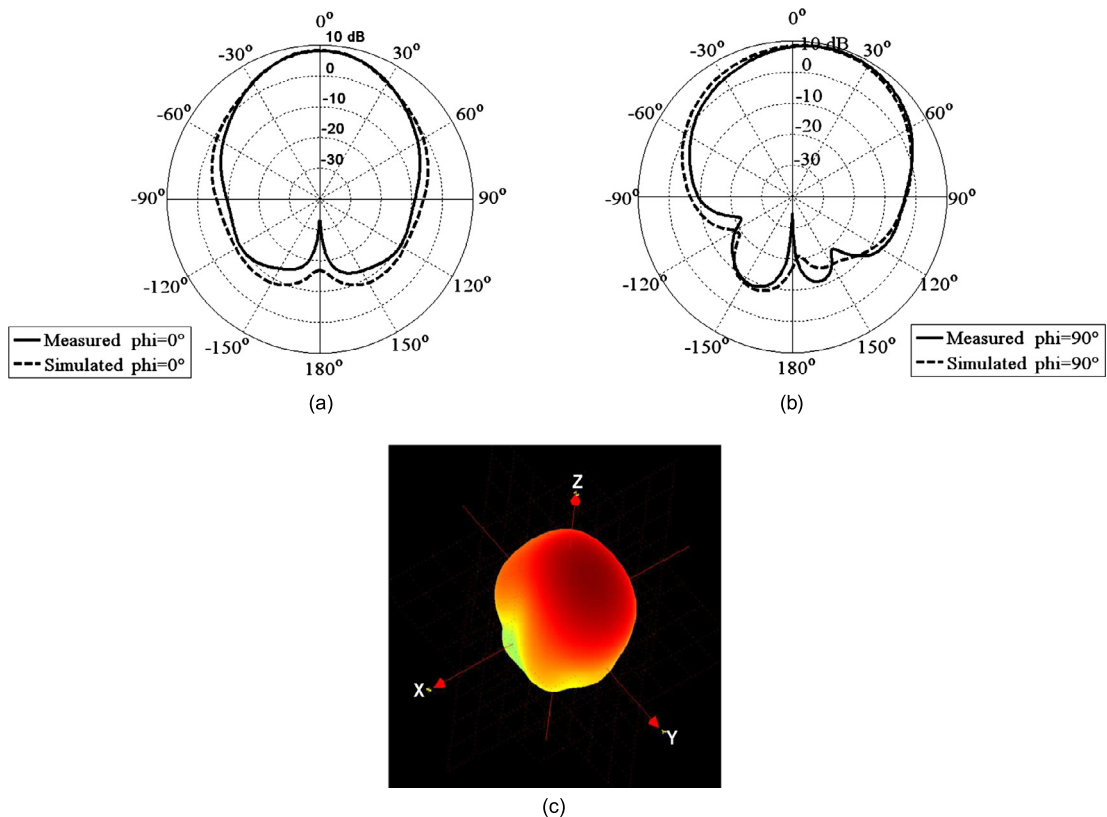
Fig. 10. (Color online.) Measured and simulated radiation patterns of the DL-HIS metamaterial antenna at $f = 1.4$ GHz, (a) H-plane, (b) E-plane and (c) measured 3D patterns.

Fig. 10. (Couleur en ligne.) Diagrammes de rayonnement obtenus par la mesure en chambre anéchoïque et par les simulations pour $f = 1,4$ GHz, (a) dans le plan H de l'antenne, (b) dans le plan E de l'antenne et (c) mesure 3D.

## 4. Radiation patterns of the designed antenna

The fabricated prototype antenna has been characterized in the anechoic chamber [20]. Fig. 10 shows the measured and simulated E- and H-plane radiation patterns at $f_0 = 1.4$ GHz. The DL-HIS antenna has an experimental maximum gain of 8.5 dB at $\vartheta = 30°$ and 5 dB in broadside ($\vartheta = 0°$). Excellent agreement is obtained between the measured and simulated results.

Table 2
DL-HIS antenna parameters.

Tableau 2
Paramètres de l'antenne DL-HIS.

a/λ_0	0.001	0.006	0.011
Bw (MHz)	≈ 140	≈ 400	≈ 400
f_0 (GHz)	1.1	1.25	1.6

Table 3
SL-HIS antenna parameters.

Tableau 3
Paramètres de l'antenne SL-HIS.

a/λ_0	0.02	0.03	0.04
Bw (MHz)	≈ 100	≈ 95	≈ 90
f_0 (GHz)	1.3	1.35	1.32
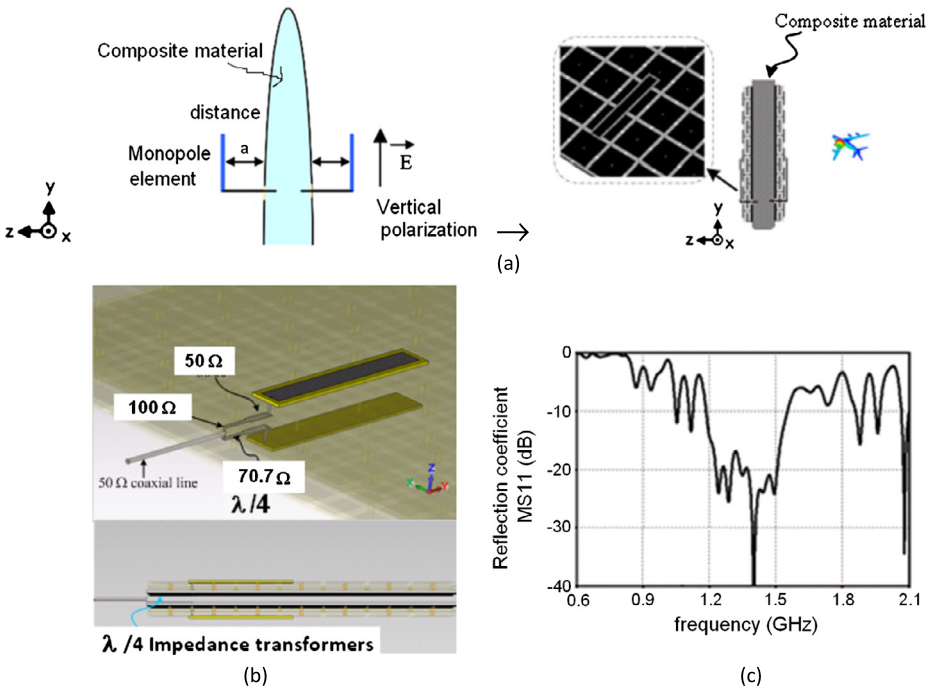
Fig. 11. (Color online.) (a) Schematic principle of the "sabre" antenna (array of two monopole antennas based on a dual-layer HIS substrate), (b) CST numerical model of the "sabre" antennal structure—the antenna is fed using a quarter-wavelength impedance transformer—and (c) the simulated reflection coefficient S_{11} (dB).

Fig. 11. (Couleur en ligne.) (a) Schéma de principe de l'antenne sabre formée d'un réseau de deux éléments monopoles placés sur deux substrats métama-tériaux (DL-HIS), (b) modélisation de la maquette numérique de l'antenne sur le logiciel CST – on voit que l'antenne est alimentée par des transformateurs d'impédance quart d'ondes – et (c) coefficient de réflexion de l'antenne sabre S_{11} (dB) obtenu par la simulation CST.

5. "Sabre" antenna

Fig. 11a shows the proposed "sabre" antenna. It consists of two arrayed monopole antennas organized on both sides of a composite material placed on the tail of an airplane. The numerical model of the "sabre" antennal structure (Fig. 11b) is performed using CST STUDIO SUITE™.

Fig. 11c shows the simulated reflection magnitude S_{11} (dB) of the antennal array. The resonant frequency is 1.4 GHz and the bandwidth is around 330 MHz: from 1.2 GHz to 1.54 GHz (relative bandwidth of 23.9%). Those results confirm the performances already obtained by the DL-HIS monopole antennas (Fig. 6 and Fig. 7).

The radiation patterns of the "sabre" antenna have been experimentally determined in both the horizontal and vertical planes for different frequencies (1.215 GHz, 1.35 GHz, and 1.45 GHz and 1.545 GHz) inside the calculated bandwidth. The results are shown in Fig. 12a–b. The array is composed only of two elements, hence the H-plane (or horizontal plane) radiation diagrams of the "sabre" antenna (Fig. 12a) are quasi-omnidirectional. The radiation diagrams are almost directive due to the suppression of the surface wave by the DL-HIS substrate.
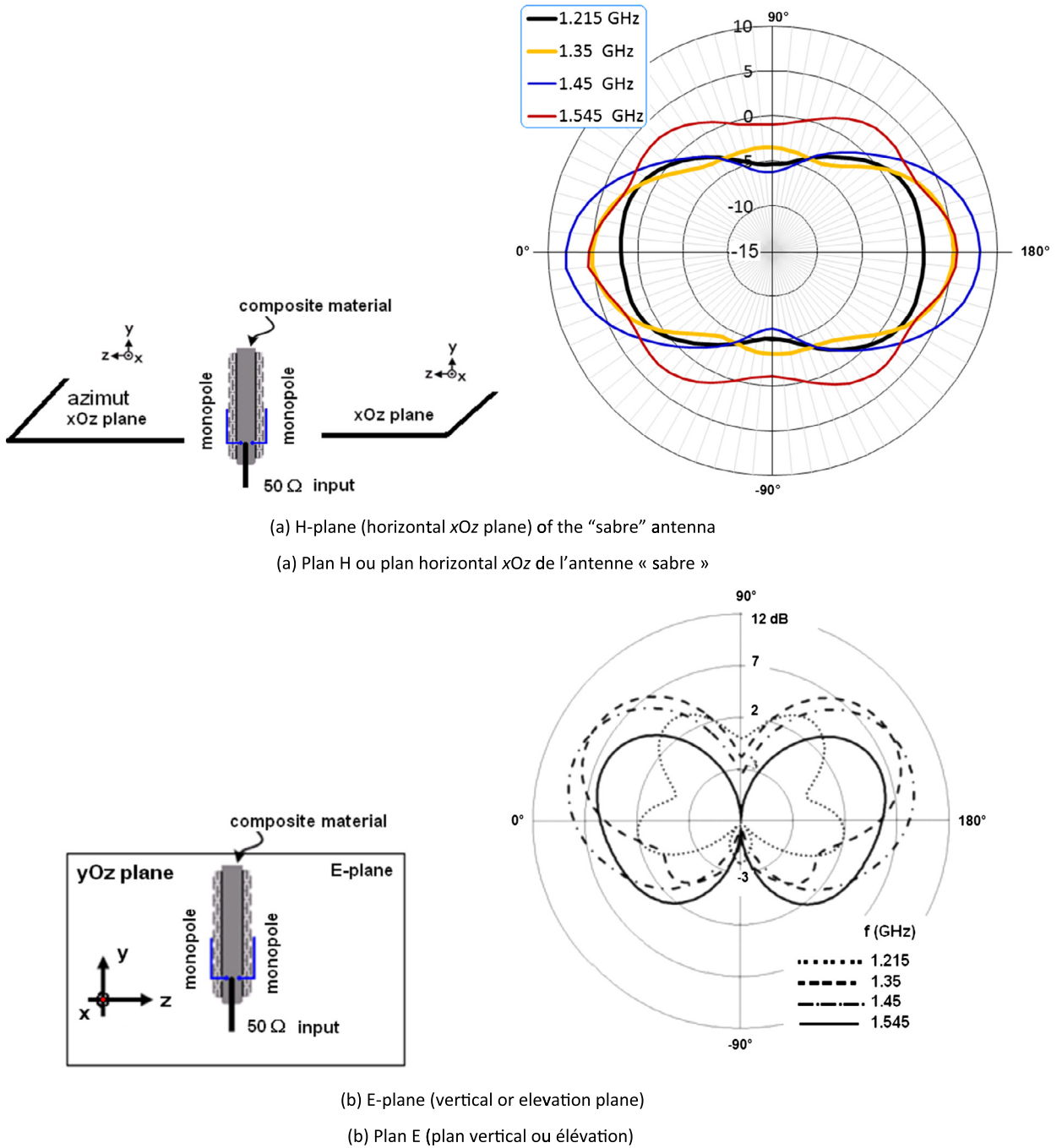
(a) H-plane (horizontal *xOz* plane) of the "sabre" antenna

(a) Plan H ou plan horizontal *xOz* de l'antenne « sabre »

(b) E-plane (vertical or elevation plane)

(b) Plan E (plan vertical ou élévation)

Fig. 12. (Color online.) Measured radiation patterns of the "sabre" antenna; (a) in the H-plane and (b) in the E-plane, for different frequencies.

Fig. 12. (Couleur en ligne.) Diagrammes de rayonnement de l'antenne sabre métamatériau mesurés pour différentes fréquences, (a) dans le plan H et (b) dans le plan E.

In the azimuth plane (E-plane or vertical plane), the radiation patterns are similar to a monopole-type antenna. The antenna gain is >2 dB over the whole operational bandwidth and is 8.2 dB at the resonant frequency.

6. Conclusion

This study shows the importance of metamaterial substrates to design low-profile (subwavelength) antennas. We present for the first time the design, optimization, and realization of a "sabre" antenna based on a compact dual-layer offset "mushroom-like" HIS structure. The advantage of the dual-layer high-impedance surfaces (DL-HIS) is the control of the

antenna's resonant frequency and VSWR bandwidth. The designed monopole antenna based on a DL-HIS substrate has a bandwidth of 24%, a gain of 8 dB at 1.4 GHz and a total thickness of $\sim\lambda_0/36$. The "sabre" antenna maintains the main properties (central frequency and the bandwidth) of the unit monopole DL-HIS antenna. It presents a vertically polarized monopole-like radiation patterns, with a maximum high gain at 1.4 GHz.

Acknowledgements

References

[1] M. Shelley, R. Pearson, J. Vazquez, Low-profile, dual-polarised antenna for aeronautical and land mobile Satcom, Int. J. Antennas Propag. (2009), http://dx.doi.org/10.1155/2009/984972, ID 984972, 6 pages.
[2] M.W. Shelley, R.A. Pearson, J. Vasquez, Low profile, dual polarised antenna for aeronautical and land mobile Satcom, in: Proc. 4th Advanced Satellite Mobile Systems Conference, ASMS '08, Bologna, Italy, ERA Technology Ltd, August 2008, pp. 16–19.
[3] M.d.C. Redondo González, Analysis of conformal antennas for avionics applications, PhD thesis, Chalmers University, January 2007.
[4] J. Verpoorte, H. Schippers, C.G.H. Roeloffzen, D.A.I. Marpaung, Smart antennas in aerospace applications, in: 2010 URSI IEEE International Symposium on Electromagnetic Theory, 2010, pp. 260–263.
[5] E. Rodriguez, O. Antreich, F. Konovaltsev, A. Philipakkis, M. Moore, D. Martel, Antenna-based multipath and interference mitigation for aeronautical applications: present and future, in: ION GNSS 2006, Fort Worth, Texas, USA, September 2006, pp. 26–29, http://www.ion.org.
[6] S. Ghosh, Thanh-Ngon Tran, Tho Le-Ngoc, A dual-layer EBG-based miniaturized patch multi-antenna structure, in: 2011 IEEE International Symposium on Antennas and Propagation, APSURSI, July 2011, pp. 1828–1831.
[7] A. Azarbar, J. Ghalibafan, A compact low-permittivity dual-layer EBG structure for mutual coupling reduction, Int. J. Antennas Propag. 2011 (June 2011), article ID 237454.
[8] N. Boisbouvier, A. Louzir, F. Le Bolzer, A.C. Tarot, K. Mahdjoubi, A double-layer EBG structure for slot-line printed devices, in: IEEE Antennas and Propagation Society International Symposium, vol. 4, 2004, pp. 3553–3556.
[9] L.-J. Zhang, C.H. Liang, L. Liang, L. Chen, A novel design approach for dual-band electromagnetic band-gap structure, Prog. Electromagn. Res. 4 (2008) 81–91.
[10] Li Yang, Mingyan Fan, Fanglu Chen, Jingzhao She, Zhenghe Feng, A novel compact electromagnetic-bandgap (EBG) structure and its applications for microwave circuits, IEEE Trans. Microw. Theory Tech. 53 (1) (2005) 183–190.
[11] M.Z. Azad, M. Ali, Novel wideband directional dipole antenna on a mushroom like EBG structure, IEEE Trans. Antennas Propag. 56 (2008) 1242–1250.
[12] M. Faisal Abedin, M. Ali, Effects of EBG reflection phase profiles on the input impedance and bandwidth of ultrathin directional dipoles, IEEE Trans. Antennas Propag. 53 (11) (2005) 3664–3672.
[13] CST MWS. Comput. Simulation Technol., Darmstadt, Germany [online] http://www.cst.com.
[14] D.F. Sievenpiper, High-impedance electromagnetic surfaces, Ph.D. dissertation, University of California, Los Angeles, USA, 1999.
[15] D. Sievenpiper, L. Zhang, R.F. Jimenez Broas, N.G. Alexopolous, E. Yablonovitch, High-impedance electromagnetic surfaces with a forbidden frequency band, IEEE Trans. Microw. Theory Tech. 47 (11) (1999) 2059–2074.
[16] D. Sieenpiper, J. Colburn, B. Fong, M. Ganz, M. Gyure, J. Lynch, J. Ottusch, J. Visher, Artificial impedance surface, 9 November 2010, U.S. Patent No. 7830310.
[17] (a) Fan Yang, Yahya Rahmat-Samii, Electromagnetic Band Gap Structures in Antenna Engineering, The Cambridge RF and Microwave Engineering Series, Cambridge University Press, Cambridge, UK, 2009, pp. 59–61, Chapter 3;
(b) Fan Yang, Yahya Rahmat-Samii, Reflection phase characterizations of the EBG ground plane for low profile wire antenna applications, IEEE Trans. Antenn. Propag. 51 (10) (2003) 2691–2703.
[18] C.M. Tran, H. Hafdallah Ouslimani, L. Zhou, A.C. Priou, High-impedance surfaces based antennas for high data rate communications at 40 GHz, Prog. Electromagn. Res. C 13 (2010) 217–229.
[19] T. Yuan, Metamaterial antennas for aeronautic applications, Ph.D. dissertation, University of Paris-Ouest–Nanterre, Nanterre, France, 2012.
[20] http://www.satimo.com/content/products/starlab.